Biochemical and Biophysical Research Communications 478 (2016) 1280–1285

Contents lists available at ScienceDirect

Biochemical and Biophysical Research Communications

journal homepage: www.elsevier.com/locate/ybbrc

Influence of αvβ3 integrin on the mechanical properties and the morphology of M21 and K562 cells

Janina R. Lange [a], Wolfgang H. Goldmann [a, *], José Luis Alonso [b]

[a] Department of Physics, Biophysics Group, Friedrich-Alexander-University Erlangen-Nuremberg, D-91052, Erlangen, Germany
[b] Department of Medicine, Mass. General Hospital, Harvard Medical School, Charlestown, MA, 02129, USA

ARTICLE INFO

Article history:
Received 2 August 2016
Accepted 17 August 2016
Available online 20 August 2016

Keywords:
αvβ3 integrin
α5β1 integrin
Microfluidics
Microconstriction assay
Cell mechanical properties
Cell morphology

ABSTRACT

Integrins play an important role in cell adhesion, morphology, migration, and many other physiological processes. The role of αvβ3 integrin has been intensively investigated in the past. However, much is still unclear about its selective role in cell contractility, adhesion, and mechanics. We looked at the influence of αvβ3 integrin on the cell mechanics of adherent M21 and suspended K562 cells with a microconstriction assay and found that the expression of αvβ3 integrin leads to higher cell stiffness and decreased fluidity in both cell lines. The disruption of the actin cytoskeleton decreased cellular stiffness in M21 (expressing α5β1 and αvβ3 integrins) and M21L (expressing only α5β1 integrin) cell lines in a similar way, but did not lead to the same baseline stiffness. The activation of integrins after the addition of Mn^{2+} led to higher stiffness in all observed cell lines, independent of αvβ3 integrin expression and disruption of the actin cytoskeleton. In summary, these results show that differences in stiffness/fluidity due to αvβ3 integrin expression or integrin activation by Mn^{2+} might not simply be explained by the coupling of integrins to actin via focal adhesions, which in turn induces changes in the actin cytoskeleton, but also by other cellular components such as the cell nucleus, intermediate filaments, or microtubules.

1. Introduction

Integrins are heterodimeric (α/β) cell adhesion receptors, expressed on the surface of most cells in the body, which consist of a bi-lobular head and two legs that span the plasma membrane [1,2]. Integrin-mediated cell adhesion controls critical signals regulating cell proliferation, differentiation, and survival [3]. They are unusual receptors as they normally exist in an inactive state, preventing cells from inappropriately adhering to each other or to the extracellular matrix (ECM). However, upon cell activation in response to a physiologic stimulus, they undergo rapid and profound reversible conformational-dependent changes in affinity, making the cells adhesive, with far-reaching consequences on cell signaling and possibly cell mechanics [2,4,5]. Further, binding of physiologic ligands and/or application of external mechanical forces cause additional changes in integrin conformation by initiating structural rearrangements in the integrin ectodomain [6,7]. The ligand-induced structural rearrangements trigger cell spreading through connections between integrin cytoplasmic tails, focal adhesion proteins, and filamentous actin, and the disruption of these processes contributes to the pathogenesis of many diseases [8,9].

αvβ3 integrin together with αIIbβ3 constitute the only known β3 integrins [1,2]. The non-covalent heterodimer of 170 kDa (αv and β3 subunits) shows wide expression, notably in endothelial cells, osteoclasts, and some solid tumors. It specifically recognizes the arginine-glycine-aspartic (RGD) tri-peptide sequence in a variety of extracellular matrix proteins, including vitronectin, osteopontin, fibrinogen, fibronectin, thrombospondin, von Willebrand factor, and cryptic collagens [10,11]. Specifically, it has been demonstrated to mediate osteoclastic bone resorption and endothelial neovascularization. Significant up-regulation of αvβ3 integrin expression has been observed in endothelial tumor as well as melanoma and glioblastoma cells [12]. Thus, αvβ3 integrin has been recognized as an important therapeutic target and antagonists to it are being explored with the aim of preventing or reversing osteoporosis, angiogenesis, and tumor regression [13]. Nevertheless, the reasons for implications of αvβ3 overexpression in tumors are widely debated and poorly understood, especially concerning cellular mechanical properties.

In our experiments, we used the microconstriction method to

* Corresponding author.
E-mail address: wgoldmann@biomed.uni.erlangen.de (W.H. Goldmann).

http://dx.doi.org/10.1016/j.bbrc.2016.08.111
0006-291X/

determine the influence of αvβ3 integrin on the mechanical properties of two cell lines [14]. Using this method, we measured the entry time, working pressure and cell size of suspended cells, or cells brought into suspension, which are flushed into micron-scaled constrictions. This allowed the calculation of the elastic stiffness and fluidity (=viscous properties) of human erythroleukemia K562 non-adherent cells, which express recombinant αvβ3 integrin (termed K562-αvβ3) [15], and human melanoma M21 adherent cells, which do no longer express αvβ3 integrin (termed M21L) after knockout [16], used as model cell lines. Both of these cell lines express other integrins, among them predominantly α5β1 integrin.

We were interested in answering the following questions: (*i*) Does the expression of αvβ3 integrin in K562/M21 cell lines, which possibly also induces changes in the cellular actin cytoskeleton due to altered linkage, result in differences in overall cell mechanical properties? (*ii*) How do the cell mechanical properties of cell lines, which express or do not express αvβ3 integrin, change when we disrupt the actin cytoskeleton? Regarding our hypothesis here are differences in stiffness only due to the actin cytoskeleton? (*iii*) Are there measurable changes in mechanical properties in these cell lines after integrin activation with Mn^{2+}? The question here pertains to whether the activation of αvβ3 and/or α5β1 integrin might increase the stiffness of the actomyosin cytoskeleton of the cell lines differently. Additionally, using morphologic analyses and flow cytometry on M21/M21L cells, we tried to explain the differences in cell mechanical properties induced by αvβ3 expression.

2. Materials and methods

2.1. Cell lines and cell culture

The human erythroleukemia cell line K562 and the transfected cell line K562-αvβ3, stably expressing recombinant αvβ3 integrin [15], as well as the human melanoma cell line M21, which constitutively expresses αvβ3, and M21L, where αvβ3 integrin was knocked out, have been described previously [16]. K562 cells were maintained in Iscove's modified Dulbecco's medium (IMDM). K562-αvβ3 cells were cultured in IMDM with G418 (1.0 mg/ml) and M21/M21L cells in RPMI 1640. All media were supplemented with 10% fetal calf serum (FCS), 2 mM L-glutamine, and 100 U/mL penicillin and streptomycin. In cellular and biochemical assays, where calcium, magnesium, or manganese cations were used, the final concentration was always 1 mM.

2.2. Cell culture reagents and antibodies

Cell culture reagents were either purchased from Invitrogen Corp. (San Diego, CA) or Fisher Scientific (Hampton, NH). Human plasma fibronectin was obtained from Sigma-Aldrich (St Louis, MO). The function-blocking and heterodimer-specific mAb LM609 against αVβ3 [17] was purchased from Millipore (Danvers, MA); αv-specific mAb 17E6 [16,18], blocking β1-specific P5D2 was from (R&D Systems, Minneapolis, MN), and APC-labeled goat anti-mouse Fc-specific antibody was from Jackson ImmunoResearch (West Grove, PA).

2.3. Flow cytometry and immunofluorescent labeling

K562 cells expressing αvβ3 were harvested by re-suspension, and M21/M21L cells by incubation in 10 mM EDTA in PBS (5 min; 25 °C) followed by washing three times in Hepes-buffered saline (20 mM Hepes, 150 mM NaCl, pH 7.4) containing bovine serum albumin (0.1% w/v) and 5 mM glucose (washing buffer, WB) [9]. About 1×10^6 cells were suspended in 100 μl WB and incubated first with each primary antibody at 10 μg/ml (30 min; 4 °C), then with APC-conjugated secondary anti-mouse Fc antibody for an additional 30 min on ice. Cells were washed in WB after each incubation, fixed in 2% paraformaldehyde, and analyzed using a BD-LSRII flow cytometer (BD Biosciences). Antibody binding to cells was expressed as mean fluorescence intensity (MFI) as determined by FlowJo software. Several times, suspended M21 and M21L cells fixed in 4% paraformaldehyde and permeabilized in 0.1% Triton solution were labeled with Alexa 488-labeled phalloidin for 30 min at RT in the dark. After WB rinsing, the cells were analyzed by flow cytometry, and the phalloidin binding was also expressed as mean fluorescence intensity (MFI). Immunofluorescent labeling of M21 and M21L cells was conducted as explained in detail in Ref. [19].

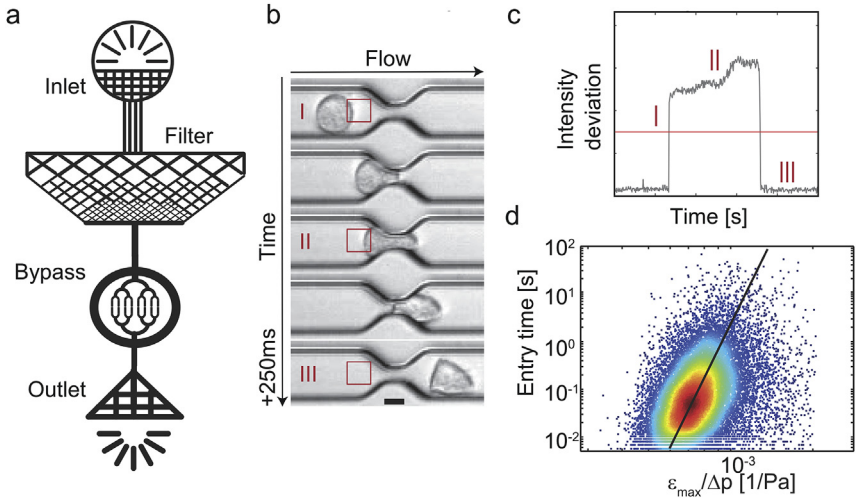

Fig. 1. (a) Schematics of the microfluidic device is shown with an inlet, debris filter, constriction area surrounded by a bypass, and outlet. The symmetric constriction area has eight parallel constrictions. (b) Sequential micrographs of a cell entering into a constriction. The red squares mark the regions of interest (ROI) for estimating the cell's entry time. Scale bar = 10 μm. (c) The entry time is calculated by thresholding the standard deviation (SD) of the pixel intensities within the ROIs (red line). Roman numbers (I–III) correspond to the numbered ROIs from (b). (d) Mechanical properties of M21 melanoma cells: scatters of $\log(t_{entry})$ vs. $\log(\varepsilon_{max}/\Delta p)$ can be fitted by a power law (double logarithmic representation). (For interpretation of the references to color in this figure legend, the reader is referred to the web version of this article.)

2.4. Cell area detection

Cell areas were calculated from fluorescence images of phalloidin-labeled cellular actin by thresholding and manual cell counting of Hoechst-stained nuclei. The sum of all pixels above an empirically found threshold (constant for all cell lines) was divided by the number of cells for each image. Error bars (standard errors, S.E.s) were calculated from n > 6 images per condition.

2.5. Microconstriction setup

The microconstriction setup and evaluation of quantitative cell mechanical properties have been described in detail in Ref. [14]. In brief, the microfluidic device consists of eight parallel constrictions connected to a single inlet and outlet with a low-resistance, pressure-equalizing bypass (Fig. 1a). The suspended cells first passed through a filter mesh before the flow was divided into eight parallel constriction branches. In each branch, the cells were squeezed through a micron-sized constriction and had to conform to the size of the constriction to pass through. The height of the device was in the range of the cell diameter (height = 17 μm for K562 cells, height = 22 μm for M21 cells), and the width and height of the constrictions were smaller than the cell diameter (height = 10 μm for K562 and 15 μm for M21 cells, width = 5 μm for both). With these dimensions, an average cell entry time between 5 and 1000 ms was achieved. The cell transit was continuously monitored by a high-speed camera (GE680, Allied Vision, Germany; 750 fps) in bright-field mode on an inverted microscope (DM-IL, Leica) with 10× magnification with a custom-written Labview-program (National Instruments).

2.6. Evaluation of mechanical properties

Image analysis was done by custom-written MatLab programs (The MathWorks). The cell entry into a constriction was analyzed from bright-field images (Fig. 1b) to measure the cell entry time t_{entry}. The standard deviation of pixel intensities of a region of interest (ROI, red squares) in front of the constrictions was used to detect the time points when the cell entered the microconstriction and when it had fully deformed to pass through the narrow channel. The signal rises (Fig. 1c) when the cell enters the constriction (Fig. 1b I), remains high as long as the cell deforms into the constriction (Fig. 1b II), and when the cell has passed through the channel, it drops immediately (Fig. 1b III).

The cell speed and cell size of the un-deformed cell were determined from the bright field images also covering the area in front of the constrictions. From the cell radius R, the maximum deformation of the cell was calculated according to $\varepsilon_{max} = (R - R_{con})/R$. The effective radius of the constriction was thereby calculated from the height h and width w of the constriction: $R_{con} = \sqrt{\frac{w*h}{\pi}}$. From the empirical relation between cell speed and flow speed, the pressure drop Δp of each constriction was calculated by Hagen-Poiseulle's law. Pressure fluctuations during a cell's transit, which are induced by other cells clogging neighboring constrictions, were continuously monitored and taken into account by Kirchhoff's circuit law [14].

To the scatter of entry time t_{entry} over the ratio of $\varepsilon_{max}/\Delta p$ a power-law relationship was fitted:

$$t_{entry} = \left(\frac{E \cdot \varepsilon_{max}}{\Delta p}\right)^{\frac{1}{\beta}}, \quad (1)$$

yielding the two fit parameters E = elastic cell stiffness and β reflecting the fluidity (=viscous behavior) of the cell population (Fig. 1d) [14]. To avoid incorrect mechanical results through strain or stress stiffening, only cells that experienced both the same pressure Δp (=stress) and the same strain (=maximum deformation ε_{max}) were compared within each plot.

Fitting was performed with a total least squares fit to scatter data of at least n > 1200 cells per measurement, combining the results of n = 3 independent measurements per condition. The data were transformed into a double logarithmic representation, allowing a linear fit to $\log(\varepsilon_{max}/\Delta p)$ and $\log(t_{entry})$. Statistics were generated by bootstrapping and the error bars indicate standard errors (S.E.s).

3. Results

To investigate differences in the mechanical properties induced by αvβ3 integrin expression, we recorded K562 and M21 cells with a high-speed camera as they entered the microconstrictions. Through power-law fitting of the scatters of $\varepsilon_{max}/\Delta p$ and t_{entry}, we calculated a cell stiffness of 1215 ± 17 Pa for M21 melanoma cells expressing α5β1 and αvβ3 integrins, while M21L cells, which only express α5β1 integrin, showed a significant reduction in stiffness to 1065 ± 17 Pa (Fig. 2a). We found inversely correlated and significantly different power-law exponents with values of 0.07 ± 0.01 for M21 and 0.09 ± 0.01 for M21L. When assessing the stiffness of wildtype K562 leukemia cells, which express only α5β1 integrin constitutively, these cells had a value of 598 ± 14 Pa, whilst the same cell type expressing α5β1 and stably transfected αvβ3 integrins showed a cellular stiffness of 655 ± 10 Pa (Fig. 2b). We calculated significantly different power-law exponents of 0.25 ± 0.01 for K562 and 0.23 ± 0.01 for K562-αvβ3 cells (p < 0.05). The expression

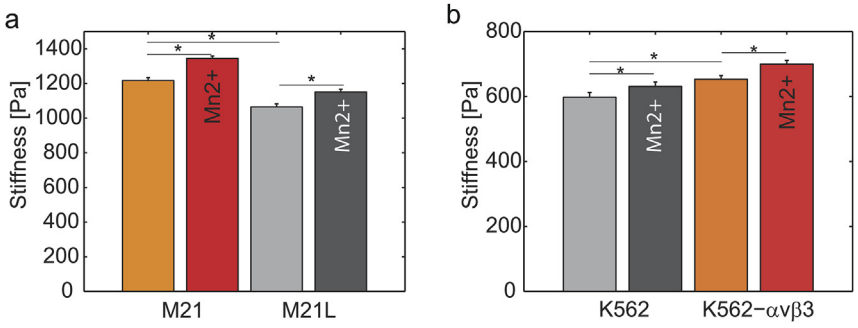

Fig. 2. Stiffness values for M21 melanoma and K562 leukemia cells expressing α5β1 and αvβ3 (M21, K562-αvβ3) or only α5β1 integrin (M21L, K562). (a) Cell stiffness for M21 cells compared to M21L cells, with/without treatment with 1 mM Mn^{2+} for 30 min n > 1200 for each population. (b) Cell stiffness for K562 cells compared to K562-αvβ3 cells, with/without treatment with 1 mM Mn^{2+} for 30 min n > 3700 for each population. In each plot, only cells that experienced the same deformation and pressure during the measurements were selected for quantitative comparison. Error bars represent S.E.s calculated by bootstrapping. Asterisks mark significant differences with p < 0.05.

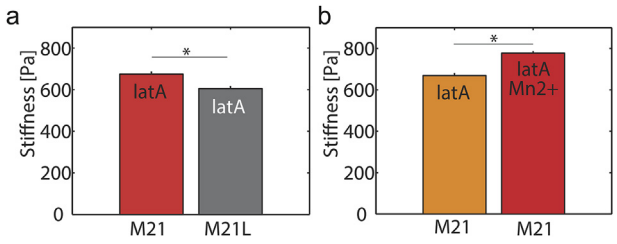

Fig. 3. Stiffness values for melanoma M21 cells that express α5β1 and αvβ3 integrins or only α5β1 integrin (M21L). (a) Cell stiffness of M21 and M21L cells after treatment with 1 μM latrunculin A for 30 min n > 4000 for each population. (b) Cell stiffness of M21 cells after treatment with 1 μM latrunculin A and after simultaneous treatment with 1 μM latrunculin A and with 1 mM Mn^{2+} for 30 min n > 4500 for each population. In each plot, only cells that experienced the same deformation and pressure during the measurements were selected for quantitative comparison. Error bars represent S.E.s calculated by bootstrapping. Asterisks mark significant differences with $p < 0.05$.

of αvβ3 integrin therefore is correlated with increased stiffness and a decreased power-law exponent in both cell lines.

Previously, it was reported that cellular stiffness is mainly determined by the concentration and mechanical tension of polymerized actin [20] and that it is probably also influenced by microtubule and/or intermediate filaments [14]. To check the influence of actin on the overall stiffness of cells with/without αvβ3 integrin expression, we treated melanoma M21 and M21L cells with 1 μM latrunculin A, a chemical agent that sequesters actin monomers in living cells [21]. We observed a stark but very similar relative reduction in cellular stiffness to 675 ± 9 Pa for M21 cells and to 604 ± 11 Pa for M21L cells (Fig. 3a) compared to their untreated counterparts (Fig. 2a). The power-law exponents rose to 0.12 ± 0.01 for M21 cells and to 0.15 ± 0.01 (significant difference) for M21L cells. The effect of the decrease in F-actin is in agreement with results from other groups, using the F-actin depolymerizing agent cytochalasin D, who also reported a dramatic decrease in cell stiffness [14,22]. Our results indicate that we cannot restore the same stiffness after the destruction of the actin cytoskeleton. In conclusion, the difference in cell stiffness might also be due to other cell components, such as microtubules, intermediate filaments, or an enhanced cell nuclear membrane.

The addition of 1 mM Mn^{2+} to the cellular medium, which is believed to activate α5β1/αvβ3 integrin mimicking inside-out activation [4], increased the stiffness in both M21 and M21L (Fig. 2a) as well as in K562 and K562-αvβ3 cell lines significantly (Fig. 2b), and markedly decreased the power-law exponents. Moreover, when the actin cytoskeleton was chemically disrupted under these conditions, we still observed a significant increase in cellular stiffness (Fig. 3b) and a significant decrease in the power-law exponent. This indicates that stiffness differences are not only induced by increased integrin-actin coupling, which presumably increases the actin content in the cells. When adding 1 mM calcium/magnesium to the cell medium, which supposedly keeps α5β1/αvβ3 integrin in an inactive/closed conformation [23], a small increase in cell stiffness was observed (data not shown). This is in accordance with previously published data, arguing that calcium/magnesium ions change the chromatin condensation, which leads to increased nuclear stiffness [24]. This points out that under these conditions, the influence of the cell nucleus dominates over the influence of integrin activation and coupling to the actin cytoskeleton. Further, the addition of 59 μg/ml fibronectin or 10 μg/ml vitronectin to the medium of M21 cells to stimulate Mn^{2+}-activated α5β1/αvβ3 integrins in their liganded state showed no increase in cellular stiffness, nor a decrease in the power-law exponent (data not shown).

We further investigated the origin of the differences in cell mechanical properties induced by αvβ3 integrin expression. Therefore, we checked the influence of integrin activation and integrin expression levels on actin as well as cell morphology, cell volume, and cell spreading area of M21 cells expressing α5β1 and αvβ3 integrins compared to M21L cells expressing only α5β1 (Fig. 4a). Finally, we also compared the actin content of both cell lines.

First, the integrin expression level of α5β1 and αvβ3 integrins in M21 and M21L cells was rechecked by flow cytometry. M21L cells express α5β1 integrin at a slightly higher level than do M21 cells, which express both α5β1 and αvβ3 integrins (Fig. 4c). K562-αvβ3 cells expressed roughly the same levels of αvβ3 and β1 integrins as M21 cells. We then analyzed cell morphology by phalloidin staining

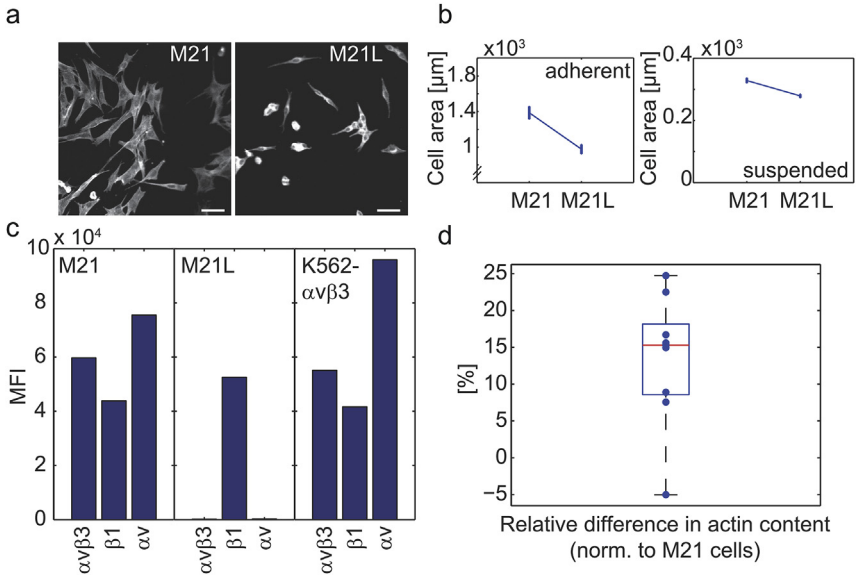

Fig. 4. a) Fluorescent phalloidin-stained M21 (expressing α5β1 and αvβ3) and M21L (only α5β1) cells, spread on 10 μg/ml fibronectin-coated surfaces for 18 h. Scale bar = 50 μm. (b) Calculated mean area of M21 and M21L cells under adherent and non-adherent conditions. Error bars represent S.E.s. (c) Integrin cell surface expression level represented by the mean fluorescent intensity (MFI), determined by flow cytometry of integrin-specific antibody labeled M21, M21L, and K562-αvβ3 cells showing αvβ3, β1, and remaining αv integrins. (d) Relative difference in actin content [%] between M21 and M21L cells, measured by flow cytometry (MFI) and normalized to M21 cells: (actin (M21) − actin (M21L))/actin (M21).

of the actin cytoskeleton. M21 cells were more spread out on fibronectin surfaces, while M21L cells had a more rounded cell body (Fig. 4a). Cell size quantification of M21 and M21L cells showed that M21 cells were larger compared to M21L cells both in the adherent (Fig. 4b left) and suspended state (Fig 4b right). This means that M21 cells had a higher cell volume. Investigations into the F-actin content in both cell lines showed an approx. 15% higher value in M21 compared to M21L cells (Fig. 4d).

4. Discussion

In this study, we could show that αvβ3 integrin expression has a systematic influence on cellular mechanics. For both M21 and K562 cell lines, an increase in cell stiffness and a decrease in cell fluidity could be correlated with the expression of αvβ3 integrin (Fig. 2a + b). This could be due to its association with the actin cytoskeleton, namely via a link between integrin, the actin cytoskeleton, and focal adhesions that leads to higher connectivity inside the cell and/or to increased actin polymerization [25,26]. Support for this notion comes from a decreased actin content measured by flow cytometry in M21L cells (Fig. 4d) compared to M21 cells and from the finding that αvβ3 integrin expressing M21 cells have a higher cell volume (Fig. 4b,c).

The disruption of the actin cytoskeleton with latrunculin A decreased the stiffness of M21 and M21L cells in the same way (Fig. 3a). This means that a difference in stiffness is still measurable between M21 and M21L cells without the influence of the actin cytoskeleton. From this it can be concluded that other cellular components such as the nucleus, microtubules, or intermediate filaments might be influenced as well by the expression of αvβ3 integrin.

Moreover, after the addition of Mn^{2+}, which is believed to activate integrin mimicking inside-out signaling, an increase in cell stiffness could be measured for all cell lines (Fig. 2a + b). Thus, this mechanism seems to be independent of αvβ3 integrin and might be promoted by other integrins. Interestingly, after the disruption of the actin cytoskeleton by latrunculin A, an increase in cell stiffness after activation through Mn^{2+} addition could be measured, which supports the notion that the cell nucleus or other cytoskeletal components might also increase the cell stiffness in the presence of manganese cations.

In the future, more detailed studies using several cell populations expressing different levels of only αvβ3 and only α5β1 will be required to finally assess the differential contribution of these integrins to integrin-mediated cellular stiffness. Unfortunately, there is no biophysical method available to date that can measure the mechanical properties of the cytoskeleton independent of the mechanics of the nucleus or vice versa, as all cell components are coupled and linked in various ways [27,28]. The best results in decoupling differential stiffnesses of cell components might be achieved by atomic force microscopy (AFM) measurements on adherent cells [29], which allows probing the mechanics of the cell periphery, or by measuring isolated cell nuclei, for example, with contact-free microfluidic measurement techniques such as optical stretcher [30]. Moreover, generating minimal cell models, which consist of only cell membranes, actin, and integrin, might help to decipher the differential contribution of α5β1 and αvβ3 integrins to bulk mechanical properties.

Acknowledgements

We thank Dr. Ben Fabry and Dr. Graeme Whyte for making the microconstriction device available for these experiments and for helpful discussions. We also thank Liz Nicholson (MA) and Victoria Jackiw, PhD for proofreading the manuscript. This work was supported by grants from the Staedlter- and Mahron-Stiftung, ANR MRSEI (France), Cure-CMD (US), German Science Foundation (DFG, FOR 1228/Z2), Research Training Group 1962 'Dynamic Interactions at Biological Membranes: From Single Molecules to Tissue' and the Emerging Fields Initiative of the University of Erlangen-Nuremberg.

Transparency document

Transparency document related to this article can be found online at http://dx.doi.org/10.1016/j.bbrc.2016.08.111.

References

[1] J.P. Xiong, T. Stehle, T. Diefenbach, R. Zhang, R. Dunker, D.L. Scott, A. Joachimiak, S.L. Goodman, M.A. Arnaout, Crystal structure of the extracellular segment of integrin alphavbeta3, Science 294 (2001) 339–345.
[2] R.O. Hynes, Integrins: bidirectional, allosteric signaling machines, Cell 110 (2002) 673–687.
[3] C.K. Miranti, J.S. Bruegge, Sensing the environment: a historical perspective on integrin signal transduction, Nat. Cell Biol. 4 (2002) E83–E90.
[4] K. Ajroud, T. Sugimore, W.H. Goldmann, D.M. Fathallah, J.P. Xiong, M.A. Arnaout, Binding affinity of metal ions to the CD11b A-domain is regulated by integrin activation and ligands, J. Biol. Chem. 279 (2004) 25483–25488.
[5] P. Roca-Cusachs, A. del-Rio, E. Puklin-Fauchner, N.C. Gauthier, N. Biais, M.P. Sheetz, Integrin-dependent force transmission to the extracellular matrix by alpha-actinin triggers adhesion maturation, Proc. Natl. Acad. Sci. U. S. A. 110 (2013) E1361–E1370.
[6] M.A. Arnaout, B. Mahalingam, J.P. Xiong, Integrin structure, allostery, and bidirectional signaling, Annu. Rev. Cell Dev. Biol. 21 (2005) 381–410.
[7] M.A. Arnaout, S.L. Goodman, J.P. Xiong, Structure and mechanics of integrin-based cell adhesion, Curr. Opin. Cell Biol. 19 (2007) 495–507.
[8] J.C. Friedland, M.H. Lee, D. Boettiger, Mechanically activated integrin switch controls alpha5beta1 function, Science 323 (2009) 642–644.
[9] J.F. Van Agthoven, J.P. Xiong, J.L. Alonso, X. Rui, B.D. Adair, S.L. Goodman, M.A. Arnaout, Structural basis for pure antagonism of integrin alphavbeta3 by a high-affinity form of fibronectin, Nat. Struct. Mol. Biol. 21 (2014) 383–388.
[10] F.P. Ross, S.L. Teitelbaum, alphavbeta3 and macrophage colony-stimulating factor: partners in osteoclast biology, Immunol. Rev. 208 (2005) 88–105.
[11] M.A. Horton, The alphavbeta3 integrin 'vitronectin receptor', Int. J. Biochem. Cell Biol. 29 (1997) 721–725.
[12] J.S. Desgrosellier, D.A. Cheresh, Integrins in cancer: biological implications and therapeutic opportunities, Nat. Rev. Cancer 10 (2010) 9–22.
[13] K. Ley, J. Rivera-Nieves, W. Sandborn, S. Shattil, Integrin-based therapeutics: biological basis, clinical use, and new drugs, Nat. Rev. Drug Discov. 15 (2016) 173–183.
[14] J.R. Lange, J. Steinwachs, T. Kolb, L.A. Lautscham, I. Harder, G. Whyte, B. Fabry, Microconstriction arrays for high-throughput quantitative measurements of cell mechanical properties, Biophys. J. 109 (2015) 26–34.
[15] J.P. Xiong, B. Mahalingham, J.L. Alonso, L.A. Borelli, S. An, B.T. Hyman, T. Rysiok, D. Mueller-Pompalla, S.L. Goodman, M.A. Arnaout, Crystal structure of the complete integrin alphavbeta3 ectodomain plus an alpha/beta transmembrane fragment, J. Cell Biol. 186 (2009) 589–600.
[16] F. Mitjans, D. Sander, J. Adan, A. Sutter, J.M. Martinez, C.S. Jaeggle, J.M. Moyano, H.G. Kreysch, J. Piulat, S.L. Goodman, An anti-alphaV-integrin antibody that blocks integrin function inhibits the development of human melanoma in nude mice, J. Cell Sci. 108 (1995) 2825–2838.
[17] D.A. Cheresh, Human endothelial cells synthesize and express an ARG-Gly-Asp-directed adhesion receptor involved in attachment to fibrinogen and von Willebrand factor, Proc. Natl. Acad. Sci. U. S. A. 84 (1987), 6571–6475.
[18] B. Mahalingam, J.F. Van Agthoven, J.P. Xiong, J.L. Alonso, B.D. Adair, X. Rui, S. Anand, M. Mehrbod, M.R. Mofrad, C. Burger, S.L. Goodman, M.A. Arnaout, Atomic basis for the species – specific inhibition of alphav integrins by monoclonal antibody 17E6 is revealed by the crystal structure of alphavbeta3 ectodomain-17E6 fab complex, J. Biol. Chem. 289 (2014) 13801–13809.
[19] C.S. Chen, J.L. Alonso, E. Ostuni, G.M. Whitesides, D.E. Ingber, Cell shape provides global control of focal adhesion assembly, Biochem. Biophys. Res. Commun. 307 (2003) 355–361.
[20] N. Wang, J.P. Butler, D.E. Ingber, Mechanotransduction across the cell surface and through the cytoskeleton, Science 260 (1993) 1124–1127.
[21] E.G. Yarmola, T. Somasundaram, T.A. Boring, I. Spector, M.R. Bubb, Actin-latrunculin A structure and function. Differential modulation of actin-binding protein function by latrunculin A, J. Biol. Chem. 275 (2000) 28120–28127.
[22] A.E. Ekpenyong, G. Whyte, K. Chalut, S. Pagliara, F. Lautenschläger, C. Fiddler, S. Paschke, U.F. Keyser, E.R. Chilvers, J. Guck, Viscoelastic properties of differentiating blood cells are fate- and function-dependent, PLoS One 7 (2012) e45237.
[23] J.L. Alonso, W.H. Goldmann, Influence of divalent cations on the cytoskeletal dynamics of K562 cells determined by nano-scale bead tracking, Biochem. Biophys. Res. Comm. 421 (2012) 245–248.
[24] K.J. Chalut, M. Höpfler, F. Lautenschläger, L. Boyde, C.J. Chan, A. Ekpenyong,

A. Martinez-Arias, J. Guck, Chromatin decondensation and nuclear softening accompany Nanog downregulation in embryonic stem cells, Biophys. J. 103 (2012) 2060–2070.
[25] W.H. Goldmann, Mechanotransduction in cells, Cell Biol. Int. 36 (2012) 567–570.
[26] W.H. Goldmann, Mechanotransduction and focal adhesions, Cell Biol. Int. 36 (2012) 649–652.
[27] Q. Guo, S.P. Duffy, K. Matthews, A.T. Santoso, M.D. Scott, H. Ma, Microfluidic analysis of red blood cell deformability, J. Biomech. 47 (2014) 1767–1776.
[28] C. Cluzel, F. Saltel, J. Lussi, F. Paulhe, B.A. Imhof, B. Wehrle-Haller, The mechanisms and dynamics of alphavbeta3 intergrin clustering in living cells, J. Cell Biol. 171 (2005) 383–392.
[29] F.M. Hecht, J. Rheinlaender, N. Schierbaum, W.H. Goldmann, B. Fabry, T.E. Schäffer, Imaging viscoelastic properties of live cells by AFM: power law rheology on the nanoscale, Soft Matter 11 (2015) 4553–4732.
[30] F. Lautenschläger, S. Paschke, S. Schinkinger, A. Breul, M. Bell, J. Guck, The regulatory role of cell mechanics for migration of differentiating myeloid cells, Proc. Natl. Acad. Sci. U. S. A. 106 (2009) 15696–15701.